

Brownian motion with dry friction: Fokker-Planck approach

Hugo Touchette, Erik Van der Straeten, and Wolfram Just

School of Mathematical Sciences, Queen Mary University of London, London E1 4NS, UK

E-mail: h.touchette@qmul.ac.uk, e.straeten@qmul.ac.uk, w.just@qmul.ac.uk

Abstract. We solve a Langevin equation, first studied by de Gennes, in which there is a solid-solid or dry friction force acting on a Brownian particle in addition to the viscous friction usually considered in the study of Brownian motion. We obtain both the time-dependent propagator of this equation and the velocity correlation function by solving the associated time-dependent Fokker-Planck equation. Exact results are found for the case where only dry friction acts on the particle. For the case where both dry and viscous friction forces are present, series representations of the propagator and correlation function are obtained in terms of parabolic cylinder functions. Similar series representations are also obtained for the case where an external constant force is added to the Langevin equation.

PACS numbers: 05.40.-a, 02.50.-r, 05.70.-a

1. Introduction

In one of his last papers, P.-G. de Gennes [1] proposed to study Brownian motion under the influence of a solid-solid or dry friction force[‡] in addition to the viscous friction force commonly studied since the works of Einstein and Langevin [3]. The main property of dry friction, as is known from common experience, is that a certain threshold force Δ_F has to be applied to a solid object resting on a solid surface in order to move the object [2]. If the applied force F is smaller than Δ_F , then the object stays at rest (stick state), whereas if $F > \Delta_F$, then the object starts moving (slip state).

The simplest way to model this behaviour mathematically is to consider a velocity-dependent force having the form $-\Delta_F\sigma(v)$, where Δ_F is a positive constant and $\sigma(v)$ stands for the sign of v with the convention $\sigma(0) = 0$. By incorporating this force into Newton's equation,

$$m\dot{v} = -\Delta_F\sigma(v) + F, \quad (1.1)$$

it is indeed easy to see that $v = 0$ is the unique attracting state when $|F| < \Delta_F$, and that $v = 0$ ceases to be attracting when $|F| \geq \Delta_F$. An object of mass m initially at rest, $v(0) = 0$, will therefore remain at rest unless an external force F greater in magnitude than the threshold or contact force Δ_F is applied.

This simple description of dry friction is commonly used in engineering and physics to study macroscopic systems in which solid-solid friction plays a significant role [4–7]. It is used, for example, to study stick-slip motion [8–11], vibrated granular

[‡] Dry friction is also called Coulomb friction [2].

media [12, 13], as well as the ratchet motion of solid objects moving on a surface which is vibrated horizontally by a time-dependent force [14] (see also [15]). In this context, de Gennes [1] proposed to study the case where the surface vibrates randomly by considering F in (1.1) to be a Gaussian white noise. Under this assumption, he derived an approximate expression for the velocity correlation function $\langle v(t)v(0) \rangle$ which generalises the well-known, exponentially-decaying velocity correlation function of the linear Langevin equation with viscous friction [3]. He also obtained the stationary velocity distribution, previously reported in [13, 16].

In this paper, we extend de Gennes's work by calculating the time-dependent propagator $p(v, t|v_0, 0)$ of the Langevin equation

$$m\dot{v} = -\alpha v - \Delta_F \sigma(v) + F + \xi(t), \quad (1.2)$$

which includes a viscous-like friction force with drag α , a dry friction force with threshold force Δ_F , a constant external force F , and a Gaussian white noise $\xi(t)$ characterised by

$$\langle \xi(t) \rangle = 0, \quad \langle \xi(t)\xi(0) \rangle = m^2 \Gamma \delta(t), \quad (1.3)$$

with $m^2 \Gamma$ the noise power. In [17, 18], the propagator of (1.2) was obtained using path integral techniques in the small-noise limit, i.e., $\Gamma \rightarrow 0$. Here we obtain the propagator without any approximation by directly solving the time-dependent Fokker-Planck equation associated with (1.2), which is explicitly given by

$$\frac{\partial p(v, t|v_0, 0)}{\partial t} = \frac{\partial}{\partial v} (\gamma v + \Delta \sigma(v) - a) p(v, t|v_0, 0) + \frac{\Gamma}{2} \frac{\partial^2 p(v, t|v_0, 0)}{\partial v^2}, \quad (1.4)$$

where $\gamma = \alpha/m$, $\Delta = \Delta_F/m$, and $a = F/m$ denote the force parameters rescaled by the mass m . To approach the solution of the Fokker-Planck equation, we first consider in section 2 the case where only dry friction is present, i.e., $\gamma = F = 0$, in order to establish the notation and to restate the results of de Gennes [1]. The effects of the viscous force is then studied in section 3. In section 4, we finally consider the case where all forces are present in order to study the stick-slip transition described above, but now in the presence of noise. We shall see there that, although there is strictly speaking no sticking in the presence of Gaussian white noise [1], the Langevin dynamics with dry friction does display two phases that resemble the stick and slip states of the noiseless dynamics.

Apart from extending de Gennes's results to include viscous damping and external forcing, the model studied here is interesting in part because it provides an example of piecewise-smooth dynamical system perturbed by noise [19] which can be solved exactly by analytical means. In the case of pure dry friction, we are indeed able to obtain closed-form expressions for the time-dependent propagator and the velocity correlation function, while for the dry-viscous and full-force cases, these functions are written in terms of spectral sums involving the so-called parabolic cylinder function. These exact results are valid for any noise power, and so also extend those obtained in [17, 18].

In a sense, it should not come as a surprise that the Fokker-Planck equation (1.4) can be solve exactly, since it is one-dimensional and piecewise linear. However, the solution is non-trivial and provides some physical insights into stick-slip transitions perturbed by noise. In particular, we are able to identify from it a number of time scales, expressed in terms of noise power and force coefficients, which could be valuable inputs for experiments on driven systems with dry friction and driven droplet dynamics, such as those performed recently by Chaudhury et al. [20–23]. Our results on the

spectrum of the Fokker-Planck operator of (1.4) also enable us to state conditions under which the viscous force can be neglected with respect to the dry friction, a regime referred to by de Gennes [1] as the partly stuck regime, or, conversely, under which dry friction can be neglected with respect to viscous friction (viscous regime). These conditions might be useful for determining whether dry friction or friction-like forces, such as liquid hysteresis [20, 21], should be considered when modeling noise-driven systems.

2. Dry friction only

We recall in this section the solution of the Fokker-Planck equation (1.4) in the simple case where there is no viscous damping and no external force, i.e., $\gamma = 0$, $a = 0$, $\Delta > 0$ and $\Gamma > 0$, for the purpose of introducing the general notation used throughout the paper and recalling the results of de Gennes [1].

The solution proceeds in the standard way (see, e.g., [24] and [25] for a rigorous but accessible account). Using the appropriate nondimensional variables

$$x = \frac{2\Delta}{\Gamma}v, \quad \tau = \frac{2\Delta^2}{\Gamma}t, \quad (2.1)$$

we first recast the Fokker-Planck equation in the form

$$\frac{\partial p(x, \tau|x', 0)}{\partial \tau} = \frac{\partial \Phi'(x)p(x, \tau|x', 0)}{\partial x} + \frac{\partial^2 p(x, \tau|x', 0)}{\partial x^2}, \quad (2.2)$$

where x' stands for the initial condition, and $\Phi(x) = |x|$ is the nondimensional potential associated with the dry friction force. The normalised stationary solution of (2.2) is given in terms of this potential by

$$\rho_*(x) = \frac{e^{-\Phi(x)}}{Z_*}, \quad (2.3)$$

where Z_* is the normalisation factor.

To find the time-dependent state $p(x, \tau|x', 0)$, we next solve the eigenvalue equation

$$-\Lambda u_\Lambda(x) = (\Phi'(x)u_\Lambda(x))' + u_\Lambda''(x), \quad (2.4)$$

for $\Lambda \geq 0$. The eigenfunctions v_Λ of the adjoint problem are related to the eigenfunctions u_Λ via the stationary distribution

$$u_\Lambda(x) = v_\Lambda(x) e^{-\Phi(x)}. \quad (2.5)$$

The two sets of eigenfunctions form a bi-orthogonal system, so that the propagator can be formally written as

$$p(x, \tau|x', 0) = \sum_{\Lambda} e^{-\Lambda\tau} u_\Lambda(x)v_\Lambda(x')/Z_\Lambda \quad (2.6)$$

with normalisation

$$Z_\Lambda = \int_{-\infty}^{\infty} v_\Lambda(x) u_\Lambda(x) dx. \quad (2.7)$$

Since we are concerned with a piecewise smooth potential whose derivative, representing the force, shows a finite jump at the origin, we have to solve (2.4) on the positive and negative domains separately, with standard, decaying boundary conditions at infinity, and then match at the origin the two solutions obtained by imposing continuity of the eigenfunction and continuity of the probability current

$$j(x) = \Phi'(x)u_\Lambda(x) + u_\Lambda'(x). \quad (2.8)$$

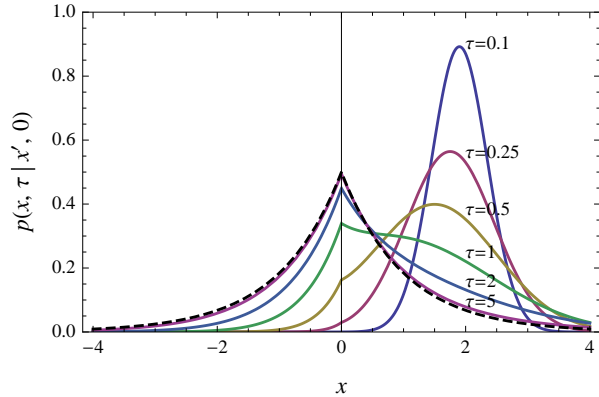


Figure 1. (Color online) Propagator $p(x, \tau | x', 0)$ of the Fokker-Planck equation for the pure dry friction case with initial condition $x' = 2$. The dashed line shows the stationary solution.

This yields the conditions

$$\begin{aligned} u_{\Lambda}(0-) &= u_{\Lambda}(0+) \\ \Phi'(0-)u_{\Lambda}(0-) + u'_{\Lambda}(0-) &= \Phi'(0+)u_{\Lambda}(0+) + u'_{\Lambda}(0+). \end{aligned} \quad (2.9)$$

To this, we also impose the initial condition $p(x, 0 | x', 0) = \delta(x - x')$.

The complete analytical solution of (2.4) with the above boundary conditions can be easily written down; see, e.g., [26] for a classical account. To keep the presentation self-contained, we summarise in Appendix A the major steps leading to the final solution given by

$$\begin{aligned} p(x, \tau | x', 0) &= \frac{e^{-\tau/4}}{2\sqrt{\pi\tau}} e^{-(|x|-|x'|)/2} e^{-(x-x')^2/(4\tau)} \\ &\quad + \frac{e^{-|x|}}{4} \left[1 + \operatorname{erf} \left(\frac{\tau - (|x| + |x'|)}{2\sqrt{\tau}} \right) \right], \end{aligned} \quad (2.10)$$

where $\operatorname{erf}(x) = 2 \int_0^x \exp(-z^2) dz / \sqrt{\pi}$ denotes the probability integral.

Figure 1 shows the behaviour of this solution as τ increases. At a qualitative level, the behaviour of $p(x, \tau | x', 0)$ shows two stages: a short time relaxation of the initial distribution towards the origin with the build-up of a corner or cusp at the origin, followed, on a longer time scale, by a build-up of the exponential tails of the stationary state $\rho_*(x)$. The first stage can be understood superficially by noting that the deterministic (zero-noise) dynamics of the model admits the solution $v(t) = v_0 - \Delta t$ with $v_0 > 0$, and thus shows a finite-time relaxation towards the fixed point $v = 0$ after a time $t_c = v_0/\Delta$. In the nondimensional variables of (2.1), this time-scale reads $\tau_c = x'$ and is the time-scale within which the propagator develops its unimodal, exponential-type shape (see figure 1).

The effect of the noise on the finite-time decay of $v(t)$ can be seen by computing the expectation of $x(\tau)$, i.e., the first moment of (2.10):

$$\begin{aligned} \langle x(\tau) \rangle &= \sigma(x') \left((|x'| - \tau) \frac{\operatorname{erfc}(-(|x'| - \tau)/(2\sqrt{\tau}))}{2} \right. \\ &\quad \left. + (|x'| + \tau) \frac{\exp(|x'|) \operatorname{erfc}((|x'| + \tau)/(2\sqrt{\tau}))}{2} \right). \end{aligned} \quad (2.11)$$

Here $\text{erfc}(x) = 1 - \text{erf}(x)$ denotes the complementary error function. If one considers cases with large initial conditions ($|x'| \gg 1$) or cases where the noise can be considered as a small perturbation, the initial stage $\tau < |x'|$ is dominated by the first contribution to (2.11), and the mean value follows the deterministic path $x' - \tau\sigma(x')$, apart from exponentially small corrections. Beyond this time scale, i.e., $\tau > |x'|$, both contributions are of the same size, and the mean value follows an exponential relaxation towards its stationary value $x_* = 0$, dominated by diffusive behaviour.

To complement this analysis, we can compute the correlation function, defined by

$$\langle x(\tau)x(0) \rangle = \int_{-\infty}^{\infty} dx \int_{-\infty}^{\infty} dx' x x' p(x, \tau|x', 0) \rho_*(x'). \quad (2.12)$$

Because of the spectral gap observed in the spectrum of the Fokker-Planck operator (see Appendix A), we know that $\langle x(\tau)x(0) \rangle$ must decay exponentially for large times; however, because of the finite-time decay of the dry friction dynamics, we expect to see corrections to this exponential decay for short times. This can be verified explicitly by computing the two integrals appearing in the expression of $\langle x(\tau)x(0) \rangle$ and by noting that the symmetric part of the propagator (2.10) does not contribute in these integrals. The result is

$$\begin{aligned} \langle x(\tau)x(0) \rangle &= \frac{e^{-\tau/4}}{\sqrt{\pi\tau}} \int_0^{\infty} dx \int_0^{\infty} dy xy e^{-(x+y)/2} e^{-(x^2+y^2)/(4\tau)} \sinh(xy/(2\tau)) \\ &= \frac{e^{-\tau/4}}{6\sqrt{\pi\tau}} \left\{ \left(\frac{\sqrt{\pi\tau}}{2} e^{\tau/4} \text{erfc}(\sqrt{\tau}/2) - 1 \right) (\tau^3 + 6\tau^2 - 12\tau + 24) + 2\tau^2 + 24 \right\} \\ &= \frac{16}{\sqrt{\pi}} \frac{e^{-\tau/4}}{(\tau/4)^{3/2}} [1 + \mathcal{O}(\tau^{-1})], \end{aligned} \quad (2.13)$$

where, in the last step, the standard asymptotic property of the probability integral was used. As usual, we can define a correlation time τ_{corr} from this result by putting the dominant exponential term in the form $e^{-\tau/\tau_{\text{corr}}}$ to obtain $\tau_{\text{corr}} = 4$ or

$$t_{\text{corr}} = \frac{2m^2\Gamma}{\Delta_F^2} \quad (2.14)$$

in the original variables given in (2.1). This correlation time and the last line of (2.13) recover the results of de Gennes [1] up to some constants.§

3. Dry and viscous friction

For the case with viscous friction, $\gamma > 0$, but without external force, $a = 0$, the appropriate nondimensional units are given by

$$x = \left(\frac{2\gamma}{\Gamma} \right)^{1/2} v, \quad \tau = \gamma t. \quad (3.1)$$

In terms of these variables, the Fokker-Planck equation (1.4) takes the form (2.2) with the potential

$$\Phi(x) = (|x| + \delta)^2/2, \quad \delta = \Delta \left(\frac{2}{\gamma\Gamma} \right)^{1/2}. \quad (3.2)$$

§ There is a typo in equation (37) of [1]: $\tau\Delta$ should be $\tau\Delta$. There also seems to be a missing factor 2 in some of de Gennes's results.

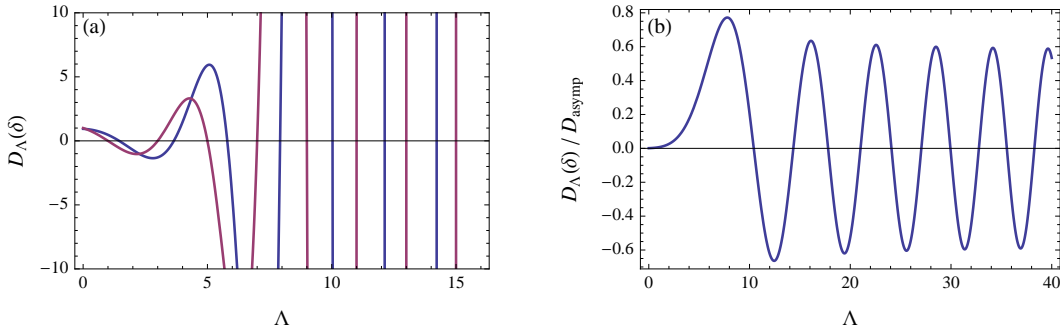


Figure 2. (Color online) (a) Parabolic cylinder function $D_\Lambda(\delta)$ as a function of the index Λ for $\delta = 0$ (purple) and $\delta = 0.5$ (blue). The zeros yield the eigenvalues $\Lambda_n^{(o)}$ which, for $\delta = 0$, are the odd positive integers. (b) Parabolic cylinder function for $\delta = 5$ normalised by the asymptotic growth $D_{\text{asyp}} = 2^{\Lambda/2}\Gamma((1 + \Lambda)/2)$ for large Λ ; see [30]. The resulting expression remains bounded.

The parameter δ measures the strength of the dry friction relative to the viscous damping and is therefore positive. However, a negative δ is possible if we have in mind to study Kramer's classical problem of a Brownian particle diffusing in a bistable or double-well potential. We will mention this case later in the paper.

Since the potential (3.2) is piecewise parabolic, the eigenvalue problem of the Fokker-Planck operator can still be solved analytically. However, to the best of our knowledge, a closed analytical expression of the propagator is not known. Various details can be found in the literature, in particular, in the context of the exit-time problem for the Ornstein-Uhlenbeck process [27] and the constrained harmonic quantum oscillator [28, 29]. As a coherent presentation cannot easily be found, we provide some details in Appendix B.

Because of the quadratic shape of the potential (3.2), we expect the spectrum to be pure point.¶ The eigenfunctions are either even or odd because of the symmetry of the potential. The eigenvalues $\Lambda_n^{(o)}$ associated with the odd eigenfunctions are determined, for $n \geq 1$, by the characteristic equation

$$D_{\Lambda_n^{(o)}}(\delta) = 0, \quad (3.3)$$

where $D_\Lambda(z)$ denotes the parabolic cylinder function [30] (see figure 2).¶ Apart from the stationary solution with eigenvalue $\Lambda_0 = 0$, the other eigenvalues associated with the even eigenfunctions are simply given by the relation

$$\Lambda_n^{(e)} = \Lambda_n^{(o)} + 1. \quad (3.4)$$

The case without dry friction, i.e., $\delta = 0$, results in a quadratic potential associated with the Ornstein-Uhlenbeck process. Even and odd eigenvalues are then given by positive even and odd integers, as the characteristic equation (3.3) reduces to an equation involving Hermite polynomials. For negative values of δ , the potential becomes bistable and the lowest non-trivial eigenvalue approaches zero, reflecting the

¶ Elliot's Theorem [25] does not apply here, so a rigorous proof of the pure point property cannot easily be given.

¶ As expected, all the eigenvalues are positive, since the parabolic cylinder function is strictly positive for negative values of the index Λ .

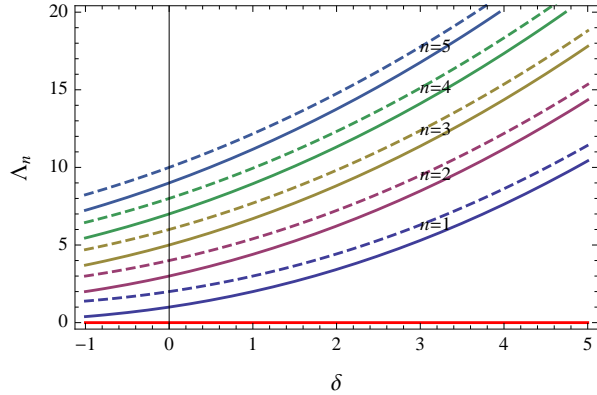


Figure 3. (Color online) Eigenvalues of the dry friction and viscous friction problem as a function of δ ; see (3.3) and (3.4). The red line corresponds to $\Lambda_0 = 0$, while the solid and dashed lines correspond, respectively, to the odd and even eigenvalues for $n = 1, 2, 3, 4$, and 5 (see also [28, 29, 31]).

behaviour of Kramer's escape rate [24]. For large positive values of δ , the spectrum develops a gap between the two lowest eigenvalues, Λ_0 and $\Lambda_1^{(o)}$, and the rest of the spectrum. These properties of the characteristic equation and of the spectrum are illustrated in figures 2 and 3.

Given the closed analytic expression of the characteristic equation, we can use standard asymptotic expansions for the parabolic cylinder function to obtain estimates for the eigenvalues [30]. In this respect, the expansion of the oscillating part of the parabolic cylinder function, e.g., in terms of Airy functions, is quite useful, as it enables us to obtain expressions for the eigenvalues for large index n and for large values of the parameter δ . For the upper part of the spectrum, we explicitly obtain

$$\Lambda_n^{(o)} \simeq (2n - 1) + \frac{2\delta}{\pi} \sqrt{2n - 1} + 2 \left(\frac{\delta}{\pi} \right)^2, \quad n \gg 1. \quad (3.5)$$

This asymptotic relation is illustrated in figure 4(a). From figure 4(c), we see that the error associated with (3.5) is of order $\mathcal{O}(n^{-1/2})$ in n . It should not come as a surprise that the leading term in (3.5) coincides with the spectrum of the Ornstein-Uhlenbeck process. However, it is not entirely obvious that the leading correction should also increase with n . Such a feature is explained by noting that the mismatch in width between the piecewise parabolic potential $\Phi(x)$ and the fully parabolic potential of the Ornstein-Uhlenbeck process increases in size when x increases.

For large values of the parameter δ and fixed value of n , the asymptotic property of the parabolic cylinder function results in

$$\Lambda_n^{(o)} + 1/2 \simeq \frac{\delta^2}{4} \left[1 + t_n \left(\frac{\delta^2}{4} \right)^{-2/3} + \frac{2t_n^2}{15} \left(\frac{\delta^2}{4} \right)^{-4/3} \right], \quad \delta \gg 1, \quad (3.6)$$

where $-t_n$ labels the zeros of the Airy function $\text{Ai}(z)$. This expression, which is illustrated in figure 4(b), captures the limit case of vanishing viscous friction and the transition from a discrete to a continuous spectrum. One clearly observes the spectral gap of size $\delta^2/4$, and the fact that the eigenvalues accumulate for large δ in a quasicontinuous way when rescaled by δ^2 to account for the different time scales defined in (2.1) and (3.1).

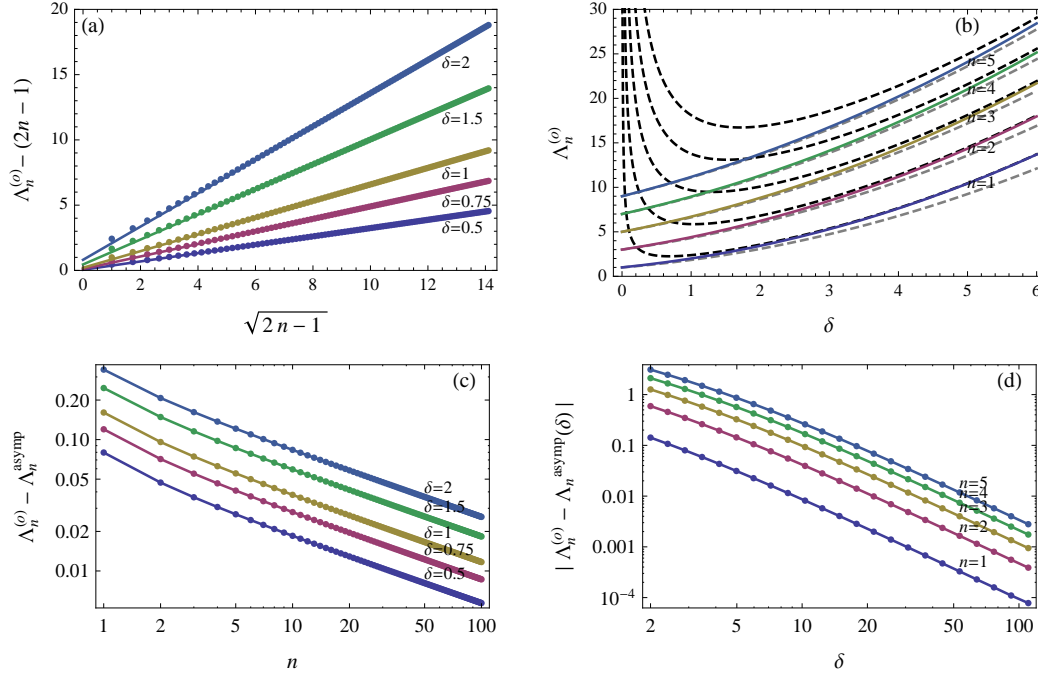


Figure 4. (Color online) Eigenvalues for the dry and viscous friction case. (a) Illustration of the asymptotic relation (lines) satisfied by $\Lambda_n^{(o)}$ (symbols) for large index n ; see (3.5). (b) $\Lambda_n^{(o)}$ (see also figure 2) as a function of δ together with the asymptotic expressions (3.5) (gray dashed line) and (3.6) (black dashed line). A crossover between the small δ (large n) and large δ (small n) asymptotics is clearly visible. (c) Log-log plot of the difference between the eigenvalue $\Lambda_n^{(o)}$ and the asymptotic expression (3.5), referred to as $\Lambda_n^{\text{asympt}}$ in the plot, as a function of n . The slope of the observed straight lines is approximately $-1/2$. (d) Log-log plot of the distance between the eigenvalue $\Lambda_n^{(o)}$ and the asymptotic expression of (3.6), referred to as $\Lambda_n^{\text{asympt}}(\delta)$ in the plot, as a function of δ . The slope of the observed straight lines is approximately -2 .

From figure 4(d), we are led to conjecture that the error term associated with (3.6) is of order $\mathcal{O}(\delta^{-2})$. Note also that if we allow for negative δ , then the asymptotic expansion of the parabolic cylinder function yields, as expected, an activation rate result for the Kramer escape problem, having the form

$$\Lambda_1^{(o)} \simeq \frac{-\delta e^{-\delta^2/2}}{\sqrt{2\pi}A(\delta)}, \quad -\delta \gg 1, \quad (3.7)$$

with the denominator of the pre-exponential factor being given by the asymptotic series⁺

$$A(\delta) = \sum_{k=0}^{\infty} \frac{(2k)!}{k!} \left(\frac{1}{2\delta^2} \right)^k \simeq -\sqrt{\pi} e^{-\delta^2/2} \frac{i\delta}{\sqrt{2}} \operatorname{erf} \left(\frac{i\delta}{\sqrt{2}} \right). \quad (3.8)$$

Having studied the spectrum of the Fokker-Planck operator in detail, we now turn to the propagator. As in the pure dry friction case, the eigenfunctions can be classified

⁺ This expression determines a nonnegative bounded real function.

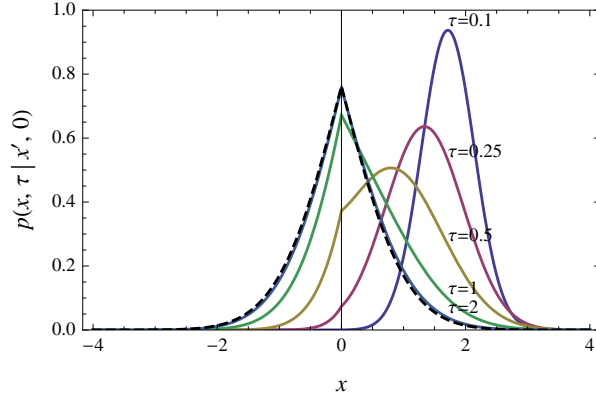


Figure 5. (Color online) Dry friction with viscous friction. Evolution of $p(x, \tau | x', 0)$ towards the stationary distribution (dashed line) as τ increases. Parameters: $x' = 2$ and $\delta = 1$. 40 modes were used to plot the propagator for the two first times; for the later times, only 5 modes were used.

as odd or even and are now given in terms of parabolic cylinder functions:

$$u_n^{(e/o)}(x) = \exp(-(x + \delta)^2/4) D_{\Lambda_n^{(e/o)}}(x + \delta), \quad x \geq 0, \quad (3.9)$$

where the expression for negative x follows by symmetry. The eigenfunctions $v_n^{(e/o)}(x)$ of the adjoint problem are, as usual, determined by (2.5). The normalisation of the odd eigenfunctions reads*

$$Z_n^{(o)} = \int_{-\infty}^{\infty} v_n^{(o)}(x) u_n^{(o)}(x) dx = 2\Lambda_n^{(o)} D_{\Lambda_n^{(o)} - 1}(\delta) \left(-\partial_{\Lambda_n^{(o)}} D_{\Lambda_n^{(o)}}(\delta) \right), \quad (3.10)$$

and yields the normalisation of the even eigenfunctions via

$$Z_n^{(e)} = \int_{-\infty}^{\infty} v_n^{(e)}(x) u_n^{(e)}(x) dx = (\Lambda_n^{(e)} + 1) Z_n^{(o)}. \quad (3.11)$$

From these expressions, we easily obtain the spectral representation of the propagator as

$$p(x, \tau | x', 0) = \rho_*(x) + \sum_{n=1}^{\infty} \exp(-\Lambda_n^{(o)} \tau) \frac{u_n^{(o)}(x) v_n^{(o)}(x')}{Z_n^{(o)}} + \sum_{n=1}^{\infty} \exp(-\Lambda_n^{(e)} \tau) \frac{u_n^{(e)}(x) v_n^{(e)}(x')}{Z_n^{(e)}}. \quad (3.12)$$

More details about this result can be found in Appendix B.

The behaviour of the propagator (3.12) for finite values of δ is illustrated in figure 5. Overall, we see that for moderate values of the viscous damping, i.e., for moderate positive values of the parameter δ , the evolution of $p(x, \tau | x', 0)$ largely resembles the case of pure dry friction with its cusp at the origin; see figure 1. The only minor difference is that $p(x, \tau | x', 0)$ converges to the stationary distribution $\rho_*(x)$ relatively

* $\partial_{\Lambda} D_{\Lambda}(\delta)$ stands for the derivative of the parabolic cylinder function with respect to its index. In addition to the standard derivation given in Appendix B, the value of the normalisation integral can be computed by comparing the exact result of the Laplace transform of the exit time distribution [27] with the Laplace transform of the odd part of the propagator shown in (3.12).

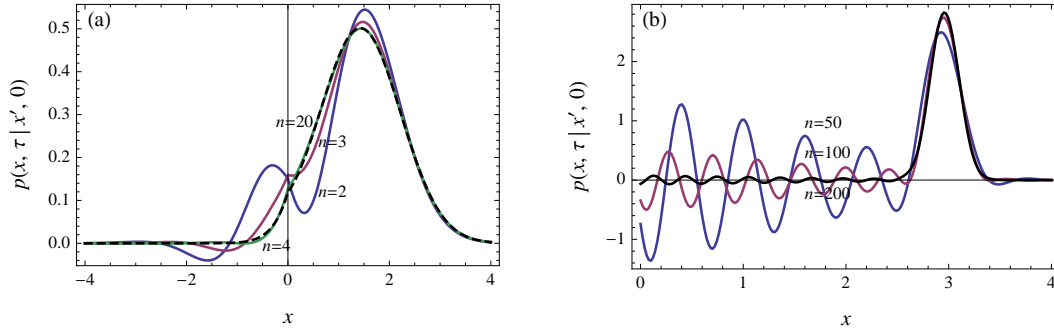


Figure 6. (Color online) Dry friction with viscous friction. (a) Convergence of the mode decomposition of $p(x, \tau | x', 0)$ for $n = 2, 3, 4$ modes (coloured lines) and $n = 20$ modes (dashed black line). Parameters: $x' = 3$, $\delta = 1$ and $\tau = 0.5$. (b) Mode convergence for short time with $n = 10, 50, 100, 200$ modes. Parameters: $x' = 3$, $\delta = 1$ and $\tau = 0.01$.

faster than with pure dry friction because of the added viscous friction. This property is reflected in the value of the lowest non-trivial eigenvalue at large δ ; see equation (3.6).

In the absence of dry friction ($\delta = 0$), the potential $\Phi(x)$ becomes quadratic and the problem reduces to the Ornstein-Uhlenbeck process, as mentioned before. In this case, the parabolic cylinder functions for integer index can be expressed in terms of Hermite polynomials

$$D_n(z) = e^{-z^2/2} \text{He}_n(z), \quad (3.13)$$

and lead to odd and even eigenvalues corresponding to odd and even positive integers, respectively (see figure 3). In this special case, the spectral decomposition (3.12) can be written in closed analytical form using Mehler's formula [25].

For the general case where dry and viscous frictions are present, we are not aware of a closed analytical expression for the propagator of (3.12). Thus, to evaluate this propagator, and to generate, for instance, the curves shown in figure 5, we have to rely on the numerical computation of the spectral sum. The behaviour of this sum as the number of eigenfunctions or modes is increased is shown in figure 6. As one expects from the result of (3.12), one requires a large number of modes to capture the short time behaviour of $p(x, \tau | x', 0)$, and a Gibbs-type phenomenon is visible when an insufficient number of modes is used. This problem becomes irrelevant when the dynamics on larger time scales is considered, as modes in the upper part of the spectrum are strongly damped.

For the correlation function, only the odd part of the propagator (3.12) contributes. Using (2.5) for the adjoint eigenfunctions and (2.3) for the stationary distribution, we obtain the representation

$$\langle x(\tau)x(0) \rangle = \sum_{n=1}^{\infty} \frac{\exp(-\Lambda_n^{(o)}\tau)}{Z_n^{(o)}} \frac{2 \left(\int_0^{\infty} x u_n^{(o)}(x) dx \right)^2}{\int_0^{\infty} \exp(-(x+\delta)^2/2) dx}. \quad (3.14)$$

The numerator of this expression can be simplified using a recurrence relation for the parabolic cylinder functions reproduced in (B.7) and (B.8), the representation (3.9) for

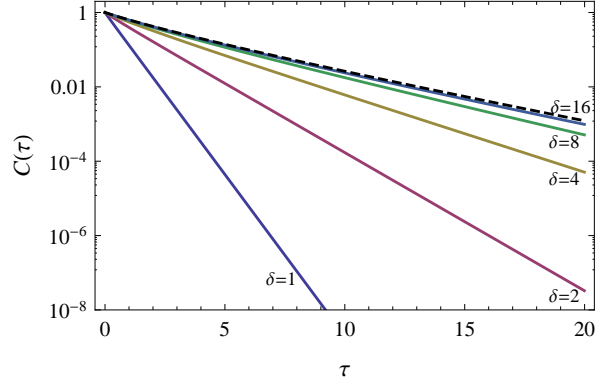


Figure 7. (Color online) Dry friction with viscous friction. Log-linear plot of the normalised correlation function $C(\tau) = \langle x(\tau)x(0) \rangle / \langle x^2 \rangle_*$ for $\delta = 1, 2, 4, 8,$ and 16 ; see (3.16). The slope of the straight lines seen in the plot defines the correlation time τ_{corr} . The dashed line corresponds to the case without viscous damping, obtained in the limit $\delta \rightarrow \infty$; see (2.13). For the purpose of comparing the dry and viscous friction case with the pure dry friction case, the data are displayed in the units defined in (2.1).

the eigenfunctions, and integration by parts to obtain

$$\int_0^\infty x u_n^{(o)}(x) dx = e^{-\delta^2/4} D_{\Lambda_n^{(o)}-2}(\delta). \quad (3.15)$$

Thus, the series (3.14) reads

$$\begin{aligned} \langle x(\tau)x(0) \rangle &= \frac{4}{\sqrt{2\pi} \operatorname{erfc}(\delta/\sqrt{2})} \sum_{n=1}^\infty \frac{\exp(-\Lambda_n^{(o)}\tau)}{Z_n^{(o)}} D_{\Lambda_n^{(o)}-2}^2(\delta) \\ &= \frac{\delta^2}{\sqrt{\pi/2} \exp(\delta^2/2) \operatorname{erfc}(\delta/\sqrt{2})} \sum_{n=1}^\infty \frac{\exp(-\Lambda_n^{(o)}\tau)}{\Lambda_n^{(o)}(\Lambda_n^{(o)}-1)^2} \frac{D_{\Lambda_n^{(o)}-1}(\delta)}{(-\partial_{\Lambda_n^{(o)}} D_{\Lambda_n^{(o)}}(\delta))}, \end{aligned} \quad (3.16)$$

where for the last step we have used (3.10) and (3.3), as well as the recurrence relation (B.14).

Figure 7 confirms that the correlation function (3.16) decays exponentially. This agrees with the spectral gap of the spectrum of the Fokker-Planck operator, which, according to equation (3.6), has a size of order $\delta^2/4$. For increasing values of δ , the correlation function of (3.16) approaches the pure dry friction result of de Gennes [1] shown in (2.13). In fact, for $\delta \sim 10$, the correlation function in the presence of dry and viscous frictions is almost indistinguishable from that obtained with dry friction only. From this, we conclude that a viscous damping of order $\gamma\Gamma \sim 0.01\Delta^2$ does not affect de Gennes's result significantly. Since this result is based on the product $\gamma\Gamma$ being small, we also conclude that de Gennes's result is a good approximation of the correlation function for the dry and viscous friction case when the noise is sufficiently weak.

The effect of viscous damping becomes apparent only at large times, as a result of the discrete spectrum obtained with dry and viscous friction. The asymptotic result of (3.6) shows that the level spacing of the eigenvalues is of order $\delta^{2/3}$, so that at a time scale of order $\tau \sim \delta^{-2/3}$, we start to see a difference between the exponential decay

of $\langle x(\tau)x(0) \rangle$ obtained with and without viscous damping. In the original units, this time scale is approximately given by

$$t \sim t_{\text{corr}}/(\gamma t_{\text{corr}})^{2/3}, \quad (3.17)$$

where t_{corr} is the correlation time of the pure dry friction case, defined before in (2.14). The influence of viscous damping on the tail of the correlation function is thus visible only if γt_{corr} is not too large. One can study this regime in more detail by using asymptotic expansions for the parabolic cylinder function in the result of (3.16).

To conclude this section, note that in the absence of dry friction, $\delta = 0$, the sum in (3.16) contains only one mode, since the numerator $D_{\Lambda_n^{(c)}-1}(0)$ vanishes for $n \geq 2$ because of the characteristic equation. This mode recovers, as expected, the correlation function of the Ornstein-Uhlenbeck process with viscous friction.

4. Constant external force

For a system with constant external force, the suitable nondimensional variables are again given by (3.1), and the potential $\Phi(x)$ which determines the drift of the Fokker-Planck equation reads

$$\Phi(x) = \frac{(|x| + \delta)^2}{2} - bx, \quad \delta = \Delta \left(\frac{2}{\gamma\Gamma} \right)^{1/2}, \quad b = a \left(\frac{2}{\gamma\Gamma} \right)^{1/2}. \quad (4.1)$$

The additional parameter b determines the strength of the ‘‘acceleration’’ a relative to the viscous damping. Depending on the relative size of the two parameters δ and b , the deterministic part of the Langevin equation (1.2) either corresponds to a particle at rest or a to moving particle, as mentioned in the introduction. For $|b| < \delta$, the deterministic steady state corresponding to the minimum of the potential (4.1) has vanishing velocity (stick state), while for $|b| > \delta$, a steady state with finite velocity occurs (slip state). In the presence of noise, these stick and slip steady states become the most probable stationary states of the Langevin dynamics, and so determine the maximum of the stationary distribution $\rho_*(x)$. This is illustrated in figure 8.

To solve the time-dependent Fokker-Planck equation for the full-force case, we proceed along the lines of the previous sections. The main steps are given in Appendix C; here we only summarise the main properties of the spectrum of the Fokker-Planck operator, the propagator $p(x, \tau|x', 0)$ and the corresponding correlation function.

Unlike the previous case where $b = 0$, eigenfunctions cannot be classified according to their symmetry when $b \neq 0$. The characteristic equation is given by

$$\Lambda_n (D_{\Lambda_n}(\delta + b)D_{\Lambda_n-1}(\delta - b) + D_{\Lambda_n}(\delta - b)D_{\Lambda_n-1}(\delta + b)) = 0. \quad (4.2)$$

Without external forcing ($b = 0$), this expression reduces of course to the case discussed in the previous section; see (3.3) and (3.4). On the other hand, without dry friction ($\delta = 0$), we end up with the integer spectrum of the Ornstein-Uhlenbeck process, since the Wronskian for the fundamental system $(D_\nu(z), D_\nu(-z))$ results in the identity [32, 33]

$$\nu D_\nu(z)D_{\nu-1}(-z) + \nu D_\nu(-z)D_{\nu-1}(z) = \sqrt{\pi}/\Gamma(-\nu). \quad (4.3)$$

Last but not least, we stress that the eigenvalues are even functions of the driving force b , since (4.2) is invariant under a change of sign. As a result, it is sufficient to consider the case of nonnegative driving b .

Figure 9 illustrates the main properties of the spectrum for fixed positive values of δ . For large forcing, i.e., in the slip phase, the spectrum approaches the integer eigenvalues

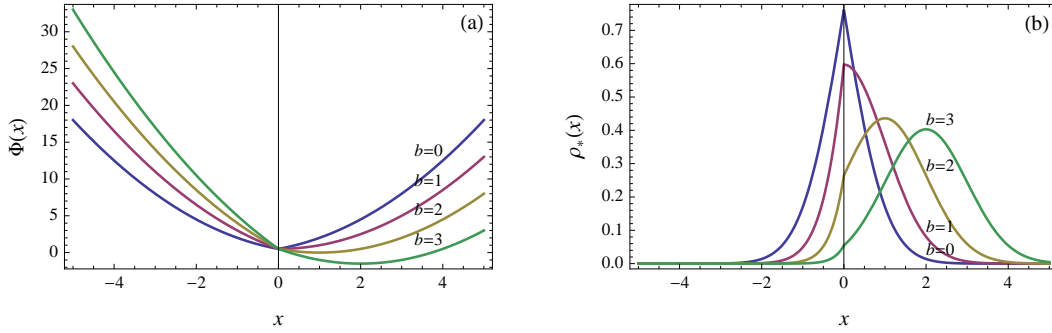


Figure 8. (Color online) Dry friction with viscous friction and forcing. (a) Potential $\Phi(x)$ as a function of x for $\delta = 1$ and for different values of b , as given by (4.1). (b) Corresponding invariant distribution, given by (2.3).

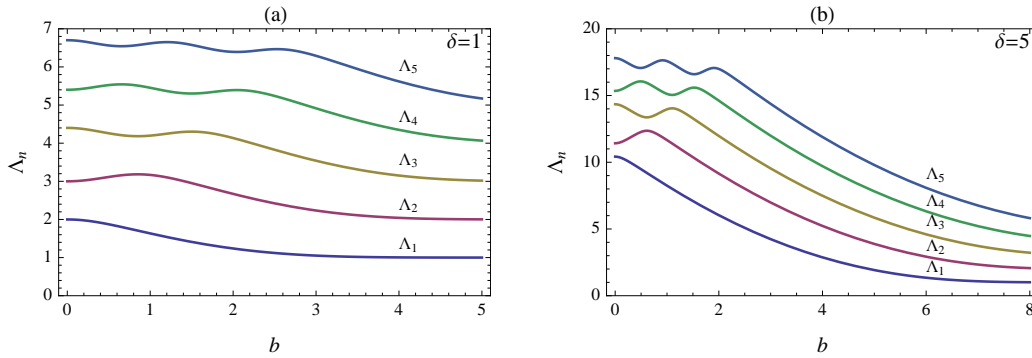


Figure 9. (Color online) Dry friction with viscous friction and forcing. First five eigenvalues Λ_n as a function of b for $\delta = 1$ (a) and $\delta = 5$ (b).

of the Ornstein-Uhlenbeck process, reflecting the parabolic minimum of the potential (see figure 8). For small forcing and relatively small viscous damping, we observe the spectral gap between the ground state and the first nonzero eigenvalue, encountered before. In the transition regime between stick and slip phase, the eigenvalues show clear oscillations and a sharp drop when the transition value $|b| = \delta$ is approached. The drop becomes more pronounced in the low noise limit, i.e., for large values of δ and b , and can be understood from (4.2) using our knowledge of parabolic cylinder functions gained in the previous section.

To be more precise, consider the stick phase, i.e., $0 \leq b < \delta$. As we have seen previously, the parabolic cylinder function $D_\Lambda(z)$ is positive if the index Λ is smaller than the lowest non-trivial eigenvalue of the corresponding undriven system, i.e., $\Lambda \lesssim z^2/4$ for large positive argument z (see figure 2). Thus all contributions to (4.2) are positive if $\Lambda \lesssim (\delta - b)^2/4$, and such a condition yields a lower bound for the lowest non-trivial eigenvalue, which determines, in turn, the parabolic shape of the spectrum in the stick phase visible in figure 9. This reasoning can be turned into an asymptotic expansion for the lowest eigenvalues if one recalls that a change in sign of one of the factors in (4.2) almost inevitably results in a zero of (4.2), given that the amplitudes

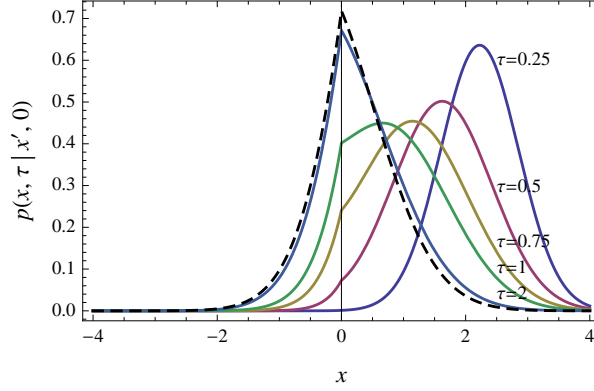


Figure 10. (Color online) Dry friction with viscous friction and forcing. Evolution of $p(x, \tau | x', 0)$ towards the stationary distribution (dashed line) as τ increases for the case where $b < \delta$. Parameters: $x' = 3$, $b = 0.5$, and $\delta = 1$.

of the terms become exponentially large.

In the slip phase $b > \delta$, the potential (4.1) has a quadratic minimum (see figure 8), and one expects the lower part of the spectrum to be of Ornstein-Uhlenbeck type. Such a feature can be derived from the characteristic equation (4.2). If the argument $\delta - b$ in (4.2) is negative, then the cylinder functions change sign at values for Λ close to even nonnegative integers (see, e.g., (3.7) for the lowest value or figure 3). Since $D_\Lambda(\delta + b)$ considerably exceeds $D_{\Lambda-1}(\delta + b)$ in magnitude, the first non-trivial root of (4.2) must then occur close to one, as observed in figure 9. By elaborating further on this argument, one can derive asymptotic expressions for the spectrum in the case $\delta > b$.

We now turn to the eigenfunctions, which for nonvanishing eigenvalues are given by the expression

$$u_n(x) = \exp(-\Phi(x)/2) \times \begin{cases} D_{\Lambda_n}(x + \delta - b), & x \geq 0 \\ \chi_n D_{\Lambda_n}(-x + \delta + b), & x \leq 0 \end{cases} \quad (4.4)$$

with the amplitude ratio

$$\chi_n = \frac{D_{\Lambda_n}(\delta - b)}{D_{\Lambda_n}(\delta + b)} = -\frac{D_{\Lambda_n-1}(\delta - b)}{D_{\Lambda_n-1}(\delta + b)}. \quad (4.5)$$

The adjoint eigenfunctions $v_n(x)$ are as usual obtained from (2.5). The normalisation (2.7) can conveniently be expressed as

$$Z_n = \Lambda_n D_{\Lambda_n}(\delta - b) D_{\Lambda_n-1}(\delta - b) \partial_{\Lambda_n} \ln \left| \frac{D_{\Lambda_n-1}(\delta - b) D_{\Lambda_n}(\delta + b)}{D_{\Lambda_n}(\delta - b) D_{\Lambda_n-1}(\delta + b)} \right|. \quad (4.6)$$

Thus, (4.4), (4.5), and (4.6) provide the required input for the propagator

$$p(x, \tau | x', 0) = \rho_*(x) + \sum_{n=1}^{\infty} \exp(-\Lambda_n \tau) \frac{u_n(x) v_n(x')}{Z_n}. \quad (4.7)$$

Figure 10 illustrates the time evolution of (4.7) in the stick phase $|b| < \delta$. Qualitatively, the dynamics is quite similar to the undriven system (see figure 5), with the difference that the symmetry of the stationary state has disappeared.

New features appear in the slip phase $b > \delta > 0$. Figure 11 shows the time evolution of the propagator with two initial conditions of opposite sign. Depending on

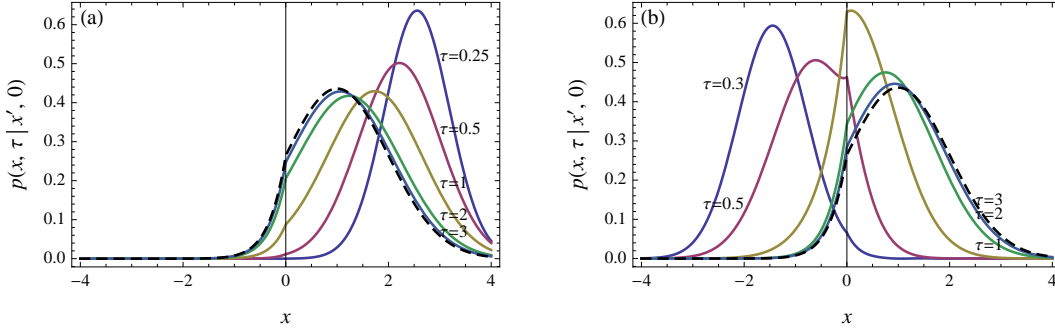


Figure 11. (Color online) Dry friction with viscous friction and forcing. Evolution of $p(x, \tau | x', 0)$ towards the stationary distribution (dashed line) as τ increases for the case where $b > \delta$ starting from $x' = 3$ (a) or $x' = -3$ (b). Parameters: $b = 2$ and $\delta = 1$.

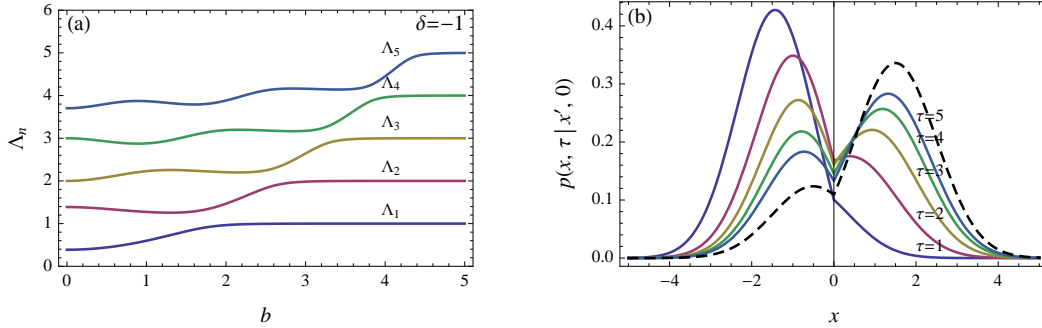


Figure 12. (Color online) Dry friction with viscous friction and $\delta < 0$. (a) First five eigenvalues as a function of b for $\delta = -1$. (b) Evolution of $p(x, \tau | x', 0)$ towards the stationary distribution (dashed line) as τ increases. Parameters: $x' = -3$, $\delta = -1$, and $b = 0.5$.

the sign of the initial condition relative to the stationary state, the propagator either remains unimodal or temporarily develops a bimodal shape. The latter is caused by a slow process near the origin, which was already responsible for the slow build-up of the tails of the stationary distribution in the undriven case.

The bimodal form of $p(x, \tau | x', 0)$ is also seen for negative values of δ , associated with Kramer's escape problem. Figure 12 gives an idea of the spectrum and the time evolution of the propagator in that case. One observes again a transition phenomenon in the spectrum when the shape of the potential changes from a bimodal to a unimodal structure. For $\delta < 0$, the driving force b affects the escape rate in the usual way. The lowest eigenvalue increases with increasing driving force as the potential barrier decreases in size. Moreover, the propagator displays, as expected, a slow tunnelling process in a double-well potential.

A few more insights into the forced case can be obtained by computing the correlation function along the lines of the previous section; see, e.g., (3.14) and (3.15).

In the present case, (4.4) yields, using (B.7) and integration by parts,

$$\begin{aligned} \int_{-\infty}^{\infty} x u_n(x) dx &= e^{-\delta^2/4} [D_{\Lambda_n-2}(\delta-b) - \chi_{\Lambda} D_{\Lambda_n-2}(\delta+b)] \\ &= \frac{2\delta e^{-\delta^2/4}}{\Lambda_n - 1} D_{\Lambda_n-1}(\delta-b), \end{aligned} \quad (4.8)$$

where for the last step the recurrence relation (B.14) and the definition (4.5) have been used. From the propagator (4.7), we then obtain

$$\begin{aligned} \langle x(\tau)x(0) \rangle - \langle x \rangle_*^2 &= \sqrt{\frac{2}{\pi}} \frac{4\delta^2}{e^{(\delta-b)^2/2} \operatorname{erfc}\left(\frac{\delta-b}{\sqrt{2}}\right) + e^{(\delta+b)^2/2} \operatorname{erfc}\left(\frac{\delta+b}{\sqrt{2}}\right)} \\ &\times \sum_{n=1}^{\infty} \frac{\exp(-\Lambda_n \tau)}{\Lambda_n (\Lambda_n - 1)^2} \frac{D_{\Lambda_n-1}(\delta-b)}{D_{\Lambda_n}(\delta-b) \partial_{\Lambda_n} \ln \left| \frac{D_{\Lambda_n-1}(\delta-b) D_{\Lambda_n}(\delta+b)}{D_{\Lambda_n}(\delta-b) D_{\Lambda_n-1}(\delta+b)} \right|}. \end{aligned} \quad (4.9)$$

In the limit $b \rightarrow 0$, this long result reduces to the correlation function of the undriven case, (3.16), as the denominator of the expansion coefficient tends towards $-2\partial_{\Lambda_n} D_{\Lambda_n}(\delta)$ and the numerator ensures that only the odd part of the spectrum contributes; see (3.4).

Figure 13 shows the plot of the correlation function normalised by the stationary variance as a function of τ and b . The red line seen in this plot marks the boundary $b = \delta$ separating the noiseless or deterministic stick and slip states. In the presence of noise, these two states are now recognisable as two different correlation phases. In the stick phase, $0 < b < \delta$, it can be shown from the spectrum of the Fokker-Planck operator that the correlation time governing the speed of the exponential decay of $\langle x(\tau)x(0) \rangle$ scales according to the law $(\delta - b)^{-2}$, and so dramatically increases near the stick-slip transition. In the slip phase ($b > \delta$), by contrast, the correlation time is mostly determined by the viscous damping, and thus does not change sensibly as a function of b . This difference in the behaviour of $\langle x(\tau)x(0) \rangle$ is clearly seen in figure 13 and becomes more visible in the small-noise limit.

5. Conclusions

In this paper we have studied a Langevin equation that includes a solid or dry friction force and an external constant force in addition to the viscous friction force commonly considered in the context of Brownian motion. This stochastic equation extends an earlier model studied by de Gennes [1], which can be thought of as describing the dynamics of a solid object resting on a tilted solid surface, which is vibrated randomly with Gaussian white noise. By solving the time-dependent Fokker-Planck equation associated with this model, we have obtained the time-dependent propagator, which gives the probability that the object has a certain velocity at any time starting from a given initial velocity, in addition to the velocity correlation function.

These results, combined with the full spectrum of the Fokker-Planck operator, allowed us to obtain a detailed understanding of dry friction in the presence of noise. In particular, we have seen that the singular nature of the dry friction force at zero velocity gives rise to a cusp in the propagator whenever the external forcing is smaller in magnitude than the dry friction force. We have also seen that the viscous damping does not alter the properties of the model much when the noise is sufficiently small, essentially because the stochastic dynamics is then confined near the origin (zero velocity state)

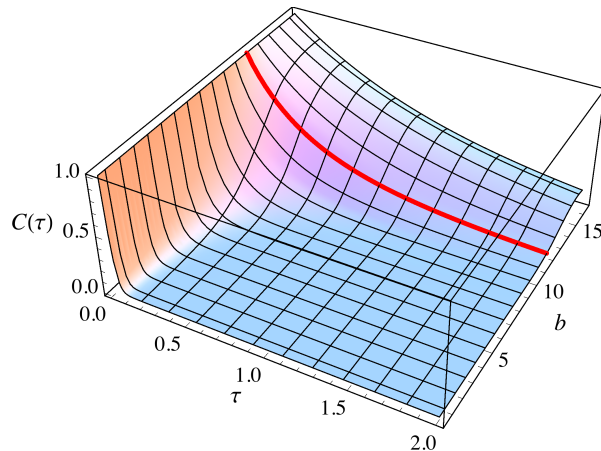


Figure 13. (Color online) Dry friction with viscous friction and forcing. Normalised correlation function $C(\tau) = (\langle x(\tau)x(0) \rangle - \langle x \rangle_*^2) / (\langle x^2 \rangle_* - \langle x \rangle_*^2)$ as a function of τ and b for $\delta = 12$. The red line at $b = \delta$ marks the transition between the stick and slip states.

which is most sensitive to dry friction. Conversely, for large noise powers, the model is mostly dominated by diffusion and behaves similarly as an Ornstein-Uhlenbeck process. Finally, we have seen that, although the stick-slip transition is blurred at the level of the stochastic dynamics, it is possible to define stick and slip phases at the level of the correlation function. The stick phase is characterized by a sharp increase of the correlation time with the external force, whereas, for the slip phase, the correlation time is mostly determined by diffusion and is almost independent of the external force. These quantitative predictions could be checked in real experiments and in more elaborate models of dry friction.

To conclude, it is worth noting that the results presented here have direct analogs in terms of quantum mechanical potentials. Indeed, some of our results about the spectrum of the Fokker-Planck operator in the presence of dry and viscous frictions can be inferred from previously-published results on the so-called constrained quantum harmonic oscillator [28, 29]. However, to the best of our knowledge, the solution that we have obtained for the full-force case has not been considered before. It might be of interest to translate this solution to the quantum context. Furthermore, it might be interesting, at least from an aesthetic point of view, to see whether the spectral sums obtained for dry and viscous forces and the full-force case can be written in closed analytical forms, as in the case of pure dry friction. We think that this should be possible given that the Fokker-Planck equation is piecewise linear in all cases.

Acknowledgments

This work was supported by an RCUK Interdisciplinary Fellowship (H.T.), and EPSRC grants nos. EP/E049257/1 (E.V.d.S.) and EP/H04812X/1 (W.J.).

Appendix A. Particle in a wedge

The stochastic dynamics of a particle in a symmetric wedge potential

$$\Phi(x) = |x| \quad (\text{A.1})$$

is a classical textbook example of a Fokker-Planck operator with spectral gap and continuous spectrum [24]. Here we recall the solution of this well-known and somewhat elementary problem, as it will certainly help the interested reader to understand the more elaborate considerations found in the other appendices.

Eigenfunctions are either even, $u_\Lambda^{(e)}(-x) = u_\Lambda^{(e)}(x)$, or odd, $u_\Lambda^{(o)}(-x) = -u_\Lambda^{(o)}(x)$, with respect to inversion. The eigenvalue equation (2.4) may be considered on the positive domain only and the boundary condition, given before in (2.9), readily reduces to

$$u_\Lambda^{(e)}(0) + \left. \frac{du_\Lambda^{(e)}(x)}{dx} \right|_{x=0} = 0, \quad u_\Lambda^{(o)}(0) = 0. \quad (\text{A.2})$$

The general solution of (2.4) can be expressed as a linear combination of exponentials. Apart from the stationary distribution (2.3) with eigenvalue $\Lambda = 0$, the solution which satisfies the symmetry, the boundary condition (A.2), and which decays to zero at infinity is given by

$$\begin{aligned} u_\Lambda^{(e)}(x) &= e^{-x/2} [2\beta_\Lambda \cos(\beta_\Lambda x) - \sin(\beta_\Lambda x)] \\ u_\Lambda^{(o)}(x) &= e^{-x/2} \sin(\beta_\Lambda x) \end{aligned} \quad (\text{A.3})$$

for $x \geq 0$, where

$$\beta_\Lambda = \sqrt{\Lambda - 1/4} > 0. \quad (\text{A.4})$$

The latter inequality determines the spectral gap and restricts the continuous spectrum to the range $\Lambda > 1/4$. As for the normalisation of the odd eigenmodes, (A.3) and (2.5) result in

$$\begin{aligned} \int_{-\infty}^{\infty} v_{\Lambda'}^{(o)}(x) u_\Lambda^{(o)}(x) dx &= \int_0^{\infty} [\cos((\beta_\Lambda - \beta_{\Lambda'})x) - \cos((\beta_\Lambda + \beta_{\Lambda'})x)] dx \\ &= 2\pi\sqrt{\Lambda - 1/4} \delta(\Lambda - \Lambda') = Z_\Lambda^{(o)} \delta(\Lambda - \Lambda'), \end{aligned} \quad (\text{A.5})$$

whereas for the even eigenmodes, we obtain

$$\begin{aligned} \int_{-\infty}^{\infty} v_{\Lambda'}^{(e)}(x) u_\Lambda^{(e)}(x) dx &= \int_0^{\infty} [(4\beta_\Lambda\beta_{\Lambda'} + 1) \cos((\beta_\Lambda - \beta_{\Lambda'})x) \\ &\quad + (4\beta_\Lambda\beta_{\Lambda'} - 1) \cos((\beta_\Lambda + \beta_{\Lambda'})x) + 2(\beta_\Lambda - \beta_{\Lambda'}) \sin((\beta_\Lambda - \beta_{\Lambda'})x) \\ &\quad - 2(\beta_\Lambda + \beta_{\Lambda'}) \sin((\beta_\Lambda + \beta_{\Lambda'})x)] dx \\ &= 2\pi(4\beta_\Lambda^2 + 1)\sqrt{\Lambda - 1/4} \delta(\Lambda - \Lambda') \\ &= Z_\Lambda^{(e)} \delta(\Lambda - \Lambda'). \end{aligned} \quad (\text{A.6})$$

The contribution of the odd eigenmodes to the propagator (2.6) can now be evaluated straightforwardly using (A.3), (2.5) and (A.5):

$$\begin{aligned} p^{(o)}(x, \tau | x', 0) &= \int_{1/4}^{\infty} e^{-\Lambda\tau} u_\Lambda^{(o)}(x) v_\Lambda^{(o)}(x') / Z_\Lambda^{(o)} d\Lambda \\ &= \frac{e^{-\tau/4} e^{-(|x|-|x'|)/2}}{2\pi} \int_0^{\infty} e^{-\beta^2\tau} [\cos(\beta(x-x')) - \cos(\beta(x+x'))] d\beta \\ &= \frac{e^{-\tau/4} e^{-(|x|-|x'|)/2}}{4\sqrt{\pi\tau}} \left(e^{-(x-x')^2/(4\tau)} - e^{-(x+x')^2/(4\tau)} \right). \end{aligned} \quad (\text{A.7})$$

For the even modes, we obtain instead

$$\begin{aligned} p^{(e)}(x, \tau|x', 0) &= \int_{1/4}^{\infty} e^{-\Lambda\tau} u_{\Lambda}^{(e)}(x) v_{\Lambda}^{(e)}(x') / Z_{\Lambda}^{(e)} d\Lambda \\ &= \frac{e^{-\tau/4} e^{-(|x|-|x'|)/2}}{2\pi} \int_0^{\infty} \frac{e^{-\beta^2\tau}}{4\beta^2+1} [(4\beta^2+1) \cos(\beta(|x|-|x'|)) \\ &\quad + (4\beta^2-1) \cos(\beta(|x|+|x'|)) - 4\beta \sin(\beta(|x|+|x'|))] d\beta. \end{aligned} \quad (\text{A.8})$$

The remaining non-trivial integrals can be evaluated using the identities [34]

$$\int_0^{\infty} e^{-\beta x^2} \sin(ax) \frac{x dx}{\gamma^2 + x^2} = -\frac{\pi}{4} e^{\beta\gamma^2} \left[2 \sinh(a\gamma) + e^{-\gamma a} \operatorname{erf}\left(\frac{2\gamma\beta - a}{2\sqrt{\beta}}\right) - e^{\gamma a} \operatorname{erf}\left(\frac{2\gamma\beta + a}{2\sqrt{\beta}}\right) \right] \quad (\text{A.9})$$

$$\int_0^{\infty} e^{-\beta x^2} \cos(ax) \frac{dx}{\gamma^2 + x^2} = \frac{\pi}{4\gamma} e^{\beta\gamma^2} \left[2 \cosh(a\gamma) - e^{-\gamma a} \operatorname{erf}\left(\frac{2\gamma\beta - a}{2\sqrt{\beta}}\right) - e^{\gamma a} \operatorname{erf}\left(\frac{2\gamma\beta + a}{2\sqrt{\beta}}\right) \right]. \quad (\text{A.10})$$

We thus end up with \ddagger

$$\begin{aligned} p^{(e)}(x, \tau|x', 0) &= \frac{e^{-\tau/4} e^{-(|x|-|x'|)/2}}{4\sqrt{\pi\tau}} \left(e^{-(x-x')^2/(4\tau)} + e^{-(x+x')^2/(4\tau)} \right) \\ &\quad - \frac{e^{-|x|}}{4} \left(1 - \operatorname{erf}\left(\frac{\tau - (|x| + |x'|)}{2\sqrt{t}}\right) \right). \end{aligned} \quad (\text{A.11})$$

The final result, (2.10), then follows from (A.7), (A.11) and

$$p(x, \tau|x', 0) = \rho_*(x) + p^{(e)}(x, \tau|x', 0) + p^{(o)}(x, \tau|x', 0). \quad (\text{A.12})$$

Appendix B. Symmetric piecewise parabolic potential

For the symmetric potential (3.2), it is sufficient to consider the eigenvalue equation (2.4) for nonnegative argument with appropriate boundary condition at the origin, since eigenfunctions are either even or odd. The boundary condition expressed in (2.9) here yields (see (A.2))

$$\delta u_{\Lambda}^{(e)}(0) + \left. \frac{du_{\Lambda}^{(e)}(x)}{dx} \right|_{x=0} = 0, \quad u_{\Lambda}^{(o)}(0) = 0. \quad (\text{B.1})$$

The differential equation (2.4) with the potential (3.2) is a special case of the so-called Kummer's equation, whose solution can be expressed in terms of Kummer functions. The solution which decays at infinity can conveniently be expressed in terms the parabolic cylinder functions. $\dagger\dagger$ To be more precise, we have that

$$u(z) = e^{-z^2/4} D_{\nu}(z), \quad (\text{B.2})$$

solves

$$u'' + (zu)' + \nu u = 0, \quad (\text{B.3})$$

\ddagger See [26] for a closely related result.

$\dagger\dagger$ We use Whittaker's notation; see, e.g., [30]

and $D_\nu(z) \sim e^{-z^2/4} z^\nu$ as $z \rightarrow +\infty$. Thus the solution of (2.4), which decays at infinity, is given by

$$u_\Lambda(x) = \exp(-(x + \delta)^2/4) D_\Lambda(x + \delta), \quad x \geq 0. \quad (\text{B.4})$$

The spectrum is now determined by the boundary condition at the origin. For the odd eigenfunctions, (B.1) and (B.4) yield the condition (3.3). If we use the following differential identity for the parabolic cylinder function:

$$D'_\Lambda(z) + \frac{z}{2} D_\Lambda(z) = \Lambda D_{\Lambda-1}(z), \quad (\text{B.5})$$

then the boundary condition for the even eigenfunctions results in

$$\Lambda_n^{(e)} D_{\Lambda_n^{(e)}-1}(\delta) = 0. \quad (\text{B.6})$$

This means that, apart from the trivial zero eigenvalue associated with the stationary state, all the other eigenvalues obey (3.4) if we take the result of (3.3) into account.

Turning now to the eigenfunctions, it should be clear that (B.4) leads to (3.9). The adjoint eigenfunctions are determined by (2.5). The orthogonality of the eigenfunctions follows from the standard differential identities for the parabolic cylinder function, which are expressed in (B.5) and can be written as

$$\frac{d \exp(-z^2/4) D_\nu(z)}{dz} = -\exp(-z^2/4) D_{\nu+1}(z) \quad (\text{B.7})$$

$$\frac{d \exp(z^2/4) D_\nu(z)}{dz} = \nu \exp(z^2/4) D_{\nu-1}(z). \quad (\text{B.8})$$

As for the normalisation, using (B.7) and (B.8), we obtain the relations

$$\frac{du_n^{(o)}(x)}{dx} = -u_n^{(e)}(x), \quad \frac{dv_n^{(e)}(x)}{dx} = \Lambda_n^{(e)} v_n^{(o)}(x), \quad (\text{B.9})$$

relating the eigenfunctions and the eigenfunctions of the adjoint problem. Integration by parts thus leads to

$$\int_0^\infty v_n^{(e)}(x) u_n^{(e)}(x) dx = \Lambda_n^{(e)} \int_0^\infty v_n^{(o)}(x) u_n^{(o)}(x) dx. \quad (\text{B.10})$$

This last equation yields (3.11). In fact, (B.9) are the remnants of the differential relations for Hermite polynomials, which guarantee that for the case $\delta = 0$, i.e., for the Ornstein-Uhlenbeck process, all eigenfunctions can be obtained by the shift operation.

To evaluate the normalisation integrals and to establish the orthogonality of eigenfunctions, we resort to a known integral identity of parabolic cylinder functions which follows from (B.7) and (B.8) using integration by parts [33]:

$$\begin{aligned} (\Lambda - \Lambda') \int_a^\infty D_\Lambda(x) D_{\Lambda'}(x) dx &= \int_a^\infty \left(\frac{d \exp(x^2/4) D_{\Lambda+1}(x)}{dx} \exp(-x^2/4) D_{\Lambda'}(x) \right. \\ &\quad \left. - \exp(x^2/4) D_\Lambda(x) \frac{d \exp(x^2/4) D_{\Lambda'+1}(x)}{dx} \right) dx \\ &= D_\Lambda(a) D_{\Lambda'+1}(a) - D_{\Lambda+1}(a) D_{\Lambda'}(a). \end{aligned} \quad (\text{B.11})$$

Choosing $a = \delta$ and $\Lambda_n^{(o)} = \Lambda \neq \Lambda' = \Lambda_m^{(o)}$, the right hand side of (B.11) vanishes due to the characteristic equation (3.3) and the left hand side results in the orthogonality condition

$$\int_{-\infty}^\infty v_m^{(o)}(x) u_n^{(o)}(x) dx = 2 \int_0^\infty D_{\Lambda_m^{(o)}}(x + \delta) D_{\Lambda_n^{(o)}}(x + \delta) dx = 0, \quad m \neq n \quad (\text{B.12})$$

for parabolic cylinder functions with index determined by (3.3). This relation is expected, as eigenfunctions are supposed to be mutually orthogonal.

To evaluate the normalisation integral, let us consider the case $a = \delta$ and $\Lambda = \Lambda_n^{(o)}$. Then (B.11) results in

$$\int_{\delta}^{\infty} D_{\Lambda_n^{(o)}}(x) D_{\Lambda'}(x) dx = D_{\Lambda_n^{(o)}+1}(\delta) \frac{D_{\Lambda_n^{(o)}}(\delta) - D_{\Lambda'}(\delta)}{\Lambda_n^{(o)} - \Lambda'} \quad (\text{B.13})$$

if we again take the characteristic equation into account. In the limit $\Lambda' \rightarrow \Lambda_n^{(o)}$, we then obtain the result (3.10) using the recurrence relation

$$z D_{\nu}(z) - D_{\nu+1}(z) - \nu D_{\nu-1}(z) = 0. \quad (\text{B.14})$$

Appendix C. Biased forcing

For the potential (4.1), the eigenvalue equation (2.4) reads

$$u_{\Lambda}''(x) + ((x \pm \delta - b)u_{\Lambda})' + \Lambda u_{\Lambda}(x) = 0, \quad (\text{C.1})$$

where the + sign applies for $x > 0$ and the - sign applies for $x < 0$. The solution that fulfills the boundary condition at infinity can be written again in terms of parabolic cylinder functions:

$$u_{\Lambda}(x) = C_{\pm} \exp(-(x \pm \delta - b)^2/4) D_{\Lambda}(\pm x + \delta \mp b), \quad x \gtrless 0. \quad (\text{C.2})$$

The boundary conditions (2.9) thus result in

$$C_- \exp(-(\delta + b)^2/4) D_{\Lambda}(\delta + b) = C_+ \exp(-(\delta - b)^2/4) D_{\Lambda}(\delta - b) \quad (\text{C.3})$$

$$C_- \Lambda \exp(-(\delta + b)^2/4) D_{\Lambda-1}(\delta + b) = -C_+ \Lambda \exp(-(\delta - b)^2/4) D_{\Lambda-1}(\delta - b). \quad (\text{C.4})$$

The condition for a non-trivial solution yields the characteristic equation (4.2). As for the amplitudes C_{\pm} , there does not seem to be a convenient form which can cope both with the limit of symmetric potentials and the different symmetries of the eigenfunctions. If we choose $C_+ = \exp(b^2/4 - \delta b/2)$, then (C.2), (C.3), and (C.4) lead to (4.4) and (4.5).

The normalisation (2.7) of the eigenfunctions (4.4) and (2.5) reads

$$\begin{aligned} Z_n &= \int_0^{\infty} D_{\Lambda_n}(x + \delta - b) D_{\Lambda_n}(x + \delta - b) dx \\ &\quad + \chi_n^2 \int_0^{\infty} D_{\Lambda_n}(x + \delta + b) D_{\Lambda_n}(x + \delta + b) dx. \end{aligned} \quad (\text{C.5})$$

Using the identity (B.11) with $a = \delta \pm b$, $\Lambda = \Lambda_n$ and $\Lambda' \rightarrow \Lambda_n$, we can express the remaining integrals in terms of parabolic cylinder functions to obtain

$$\begin{aligned} Z_n &= D_{\Lambda_n+1}(\delta - b) \partial_{\Lambda_n} D_{\Lambda_n}(\delta - b) - D_{\Lambda_n}(\delta - b) \partial_{\Lambda_n} D_{\Lambda_n+1}(\delta - b) \\ &\quad + \chi_n^2 [D_{\Lambda_n+1}(\delta + b) \partial_{\Lambda_n} D_{\Lambda_n}(\delta + b) - D_{\Lambda_n}(\delta + b) \partial_{\Lambda_n} D_{\Lambda_n+1}(\delta + b)] \end{aligned} \quad (\text{C.6})$$

Using the identity (B.14) to eliminate the cylinder functions with the largest index, $D_{\Lambda_n+1}(\delta \pm b)$, and applying the definition (4.5), we finally arrive at the result of (4.6).

References

- [1] P.-G. de Gennes. Brownian motion with dry friction. *J. Stat. Phys.*, 119(5):953–962, 2005.
- [2] F. P. Bowden and D. Tabor. *Friction and Lubrication of Solids*. Oxford University Press, Oxford, 1950.
- [3] C. W. Gardiner. *Handbook of Stochastic Methods for Physics, Chemistry and the Natural Sciences*, volume 13 of *Springer Series in Synergetics*. Springer, New York, 2nd edition, 1985.
- [4] H. Olsson, K. J. Aström, C. Canudas de Wit, M. Gäfvert, and P. Lischinsky. Friction models and friction compensation. *Eur. J. Control*, 4(3):176–195, 1998.
- [5] B. N. J. Persson. *Sliding Friction: Physical Principles and Applications*. Springer, Berlin, 1998.
- [6] J.-C. Piedboeuf, J. de Carufel, and R. Hurteau. Friction and stick-slip in robots: Simulation and experimentation. *Multibody Sys. Dyn.*, 4(4):341–354, 11 2000.
- [7] E. J. Berger. Friction modeling for dynamic system simulation. *Appl. Mech. Rev.*, 55(6):535–577, 2002.
- [8] F.-J. Elmer. Nonlinear dynamics of dry friction. *J. Phys. A: Math. Gen.*, 30(17), 1997.
- [9] R. I. Leine, D. H. van Campen, A. de Kraker, and L. van den Steen. Stick-slip vibrations induced by alternate friction models. *Nonlin. Dyn.*, 16(1):41–54, 05 1998.
- [10] Q. Feng. A discrete model of a stochastic friction system. *Comp. Methods Appl. Mech. & Eng.*, 192(20-21):2339–2354, 2003.
- [11] G. J. Stein, R. Zahoransky, and P. Mucka. On dry friction modelling and simulation in kinematically excited oscillatory systems. *J. Sound and Vibration*, 311(1-2):74–96, 2008.
- [12] Y. Murayama and M. Sano. Transition from Gaussian to non-Gaussian velocity distribution functions in a vibrated granular bed. *J. Phys. Soc. Jap.*, 67(6):1826–1829, 1998.
- [13] A. Kawarada and H. Hayakawa. Non-Gaussian velocity distribution function in a vibrating granular bed. *J. Phys. Soc. Jap.*, 73(8):2037–2040, 2004.
- [14] A. Buguin, F. Brochard, and P. G. de Gennes. Motions induced by asymmetric vibrations. *Eur. Phys. J. E*, 19(1):31–36, 2006.
- [15] D. Fleishman, Y. Asscher, and M. Urbakh. Directed transport induced by asymmetric surface vibrations: making use of friction. *J. Phys.: Cond. Matter*, 19(9), 2007.
- [16] H. Hayakawa. Langevin equation with Coulomb friction. *Physica D*, 205(1-4):48–56, 2005.
- [17] A. Baule, E. G. D. Cohen, and H. Touchette. A path integral approach to random motion with nonlinear friction. *J. Phys. A: Math. Theor.*, 43(2):025003, 2010.
- [18] A. Baule, E. G. D. Cohen, and H. Touchette. Stick-slip motion of solids with dry friction subject to random vibrations and an external field. 2010. In preparation.
- [19] M. di Bernardo, C. J. Budd, A. R. Champneys, and P. Kowalczyk. *Piecewise-Smooth Dynamical Systems: Theory and Applications*. Springer, New York, 2008.
- [20] S. Daniel and M. K. Chaudhury. Rectified motion of liquid drops on gradient surfaces induced by vibration. *Langmuir*, 18(9):3404–3407, 2002.
- [21] M. K. Chaudhury and S. Mettu. Brownian motion of a drop with hysteresis dissipation. *Langmuir*, 24:6128–6132, 2008.
- [22] P. S. Goohpattader, S. Mettu, and M. K. Chaudhury. Experimental investigation of the drift and diffusion of small objects on a surface subjected to a bias and an external white noise: Roles of Coulombic friction and hysteresis. *Langmuir*, 25(17):9969–9979, 2009.
- [23] P. S. Goohpattader and M. K. Chaudhury. Diffusive motion with nonlinear friction: Apparently Brownian. *J. Chem. Phys.*, 133:024702, 2010.
- [24] H. Risken. *The Fokker-Planck Equation: Methods of Solution and Applications*. Springer, Berlin, 1989.
- [25] W. Horsthemke and R. Lefever. *Noise-Induced Transitions*. Springer, Berlin, 1984.
- [26] E. Wong. The construction of a class of stationary Markoff processes. In R. Bellman, editor, *Stochastic Processes in Mathematical Physics and Engineering*, page 264, Providence, R.I., 1964. American Mathematical Society.
- [27] A. J. F. Siegert. On the first passage time probability problem. *Phys. Rev.*, 81(4):617, 1951.
- [28] P. Dean. The constrained quantum mechanical harmonic oscillator. *Proc. Cambridge Phil. Soc.*, 62:277, 1966.
- [29] F. C. Auluck and D. S. Kothari. The quantum mechanics of a bounded linear harmonic oscillator. *Math. Proc. Cambridge Phil. Soc.*, 41(02):175–179, 1945.
- [30] M. Abramowitz and I. A. Stegun. *Handbook of Mathematical Functions*. Dover, New York, 1970.
- [31] L. M. Riccardi and S. Sato. First-passage-time density and moments of the Ornstein-Uhlenbeck process. *J. Appl. Prob.*, 25:43, 1988.
- [32] W. Magnus, F. Oberhettinger, and R. P. Soni. *Formulas and Theorems for the Special Functions*

of Mathematical Physics. Springer, Berlin, 1966.

[33] H. Buchholz. *The Confluent Hypergeometric Function*. Springer-Verlag, Berlin, 1969.

[34] I. S. Gradshteyn and I. M. Ryzhik. *Table of Integrals, Series, and Products*. Academic Press, New York, 1980.